Effect of the low constituent boron on martensitic transformation, magnetic, and magnetocaloric properties of $Ni_{50}Mn_{35}In_{15}$ Heusler alloys

M. M. Cicek,[1] S. Saritas,[1] O. Yildirim,[2] and B. Emre[1,*]

[1] *Department of Engineering Physics, Faculty of Engineering, Ankara University, Ankara 06100, Turkey*
[2] *Empa-Swiss Federal Laboratories for Material Science and Technology, CH-8600 Dübendorf, Switzerland*

We report the structural, magnetic, and magnetocaloric properties $Ni_{50}Mn_{35-x}B_xIn_{15}$ (x=1,1.5) Heusler alloys by using room-temperature X-ray diffraction (XRD), differential scanning calorimetry (DSC), and magnetization measurements. The substitution of B instead of Mn decreases the transition temperatures. Moreover, we observe a large magnetization difference between austenite and martensite phases with a thermal hysteresis around the martensitic transition. Magnetic field dependent measurements reveal that the application of a magnetic field stabilizes the austenite phase, which has higher magnetization. We calculate magnetic entropy change by two methods, namely, Maxwell relation and fraction method. We computed a maximum magnetic entropy change of 15 J $kg^{-1}K^{-1}$ and 8 J $kg^{-1}K^{-1}$ around magnetostructural phase transition for a magnetic field change of 5 T, respectively, for $Ni_{50}Mn_{34}B_1In_{15}$ and $Ni_{50}Mn_{33.5}B_{1.5}In_{15}$ samples.

I. INTRODUCTION

Refrigeration has become one of the main demands of the human being's daily life. The universal spread of refrigerators, air conditioners leads to enormous energy consumption. Besides, according to the report of the International Energy Agency (IEA), the use of energy for space cooling is growing faster than for any other end users in buildings[1,2]. The rapid increase in energy demand for refrigeration will lead to an energy crisis called 'cold crunch'[1]. Thereby, the steps to prevent such a crisis is a hot topic for a wide range of scientist and researchers. From material science point of view, caloric cooling based on caloric effects is a promising step to meet the energy efficiency requirements. Caloric effects occur in many materials due to entropy changes induced by external fields that are named according to these external fields. Hence, inducing the entropy changes through magnetic, pressure, uniaxial stress and electric field named as magnetocaloric, barocaloric, elastocaloric and electrocaloric effects, respectively.

NiMn-based magnetic shape memory alloys (MSMAs) have been widely studied from different perspectives such as: caloric effects[3–6], magnetic shape memory effect[7–9], magnetoresistance[10,11], magnetothermal conductivity[12], and the conventional shape memory effect[13–15]. Generally, these compounds show a martensitic transition which is a first order temperature-induced structural phase transition between a high temperature cubic ferromagnetic austenitic phase and a low temperature weakly magnetic martensitic phase. This transition is therefore clasified as magnetostructural phase transition (MST). A jump-like change in magnetization is the main driving force for the magnetic field-induced martensitic phase transformation. It is reported that specific features of the electronic band structures of the Heusler alloys are responsible for the MSTs[16]. Therefore, the change related to electronic band structure such as the alloy composition, the concentration of valence electrons per atom (e/a), interatomic distances, and crystal structure homogeneity will affect the phase transitions and related phenomena[17].

Among the series of Ni-Mn based Heusler alloys, off-stoichiometric alloys of Ni-Mn-In Heusler systems are subject of interest due to the coexistence of structural and magnetic phase transitions, which allows these materials promising candidates for applications with exhibiting a wide range of properties such as giant normal and inverse magnetocaloric effect[17–21], giant magnetoresistance[22,23], Hall effect[24], and magnetic shape memory effect[25]. The aforementioned properties are extremely sensitive to their stoichiometry, thus, several studies have been focused on the phase transformation characteristics by either changing the composition or chemical substitution in Ni-Mn-In alloys[5,17,26]. The magnetic interactions in Ni-Mn-In alloys showed Rudermann-Kittel-Kasuya-Yoshida type exchange interactions among the Mn atoms that sustain the ferromagnetism in austenite phase, which also lead foregoing effects. The structural instability of austenite phase is maintained by the redistrubition of antiferromagnetically interacted 3d-electrons ensued from the Ni and Mn atoms at In sides[27,28]. Therefore, the substitution of elements with different valence electrons can affects the properties of phase transitions, which is mediated through the interactions among the 3d-electrons.

In this task, theoretical studies proposed that substitution of the nonmagnetic element instead of Mn, that might be beneficial to reach the enhanced magnetocaloric properties, resulting in decreased the magnetic exchange interactions[29]. There exist some experimental reports in which only Cu or Al substituted for Mn in Ni-Mn-In alloys[26,30–32]. Among the all elements, boron is an attractive dopant due to the smallest ionic radius compared to that of other group III-elements, and it is studied in several works as an isoelectronic substitution instead of In in Ni-Mn based alloys[17,20,33–35]. In addition, to the best of our knowledge, there is no experimental study investigating the B substitution instead of Mn in Ni-Mn-In alloys. Thereby, in study we focused

This document is the accepted manuscript version of the following article:
Cicek, M. M., Saritas, S., Yildirim, O., & Emre, B. (2020). Effect of the low constituent boron on martensitic transformation, magnetic, and magnetocaloric properties of Ni50Mn35In15 Heusler alloys. Journal of Alloys and Compounds, 155493 (17 pp.).
https://doi.org/10.1016/j.jallcom.2020.155493

on and reported the of effect of B substitution instead of Mn side, on the the martensitic transition characteristics, thermomagnetic, and magnetocaloric properties of $Ni_{50}Mn_{35-x}B_xIn_{15}$ (x=1,1.5) alloys.

II. METHODS

The ingots of polycrystalline $Ni_{50}Mn_{35-x}B_xIn_{15}$ (x=1, 1.5) were fabricated by arc melting under argon atmosphere. Hereafter, samples will be refered as B1 and B1.5 based on their x values. The excess of Mn 3%wt was added to compensate for the Mn evaporation during the melting procedure. The samples were re-melted in several times with flipped between the meltings to reach better homogeneity. The obtained amount of each ingots weight loss was less than 1 % of the total weight after melting. To better homogeneity, the piece of ingots were sealed in quartz tube under argon atmosphere annealed at 1073 K for 1 week. The structural characterization was measured at room temperature by X-ray powder diffraction with Mo K_α radiation, where the observed patterns were refined by the Rietveld method using the FullProf program package[36]. Differential scanning calorimetry (DSC) was performed using a HITACHI 7020 Model[37] . The temperature was swept at 10 K min^{-1} between 175 K and 350 K. The total entropy changes (ΔS) were calculated using the relation of ΔS=L/T_M, where L is the latent heat and T_M is the magnetostructural phase transformation temperatures estimating from the peak positions in the DSC heat flow curves. The magnetization measurements were performed by using a Quantum Design physical properties measurement system (PPMS), equipped with a vibrating sample magnetometer (VSM) option[37]. The samples weighted before the measurements on a sensitive scale (10^{-5} gram) and placed into capsules and measured with a contamination free half-cylinder brass sample holder. Prior to the temperature dependent magnetization measurements (M(T)), the samples were prepared by cooling down to 10 K in the absence of the magnetic field. Then the magnetic field was applied and temperature was increased to the 400 K where the data is taken subsequently during cooling (FC) and heating (FH) direction without removing the magnetic field. The rates of temperature variation was limited to 2 K/min to eliminate the instrumental lag caused by the thermal heterogeneity in the sample. The magnetic field dependent magnetization curves (M(H)) were performed with a magnetic field up to the 5 T with adopting M-H loop process[38] and the magnetic field was swept at a rate of 0.05 T/s. The M(H) curves were carried out first samples were initially cooled down to the martensitic transformation temperature in zero magnetic field then the sample heated up to the desired temperatures. The data was recorded during several cycles of increasing and decreasing field.

III. RESULTS AND DISCUSSION

The powder X-rays diffraction profiles have showed in Fig 1, which were recorded at room temperature. The patterns were refined by the Rietveld refinement and where the results have shown in Table 1. According to the XRD data shows that both alloys have displayed as a mixture of cubic austenite $L2_1$ structure (space group Fm-3m) and tetragonal martensite $L1_0$ structure (space group I4/mmm). During the refinement, boron atoms are treated as interstitial atoms, for instance, the Mn and Ni atoms are occupied the 4a and 8c Wykoff positions in the cubic phase, respectively. The excess Mn atoms occupy randomly at the In (4b) site. The results have given in Table 1, where the quality of refinements are ascribed by the R_p and R_{wp} and also the goodness of the fit of the models was assessed by calculating χ^2. The lattice parameters have tended to decrease in cubic and martensite phase with the addition of B instead of Mn due to lower atomic radius of B as compared to Mn. Moreover, our results in line with the similar alloys reported previously[17,35].

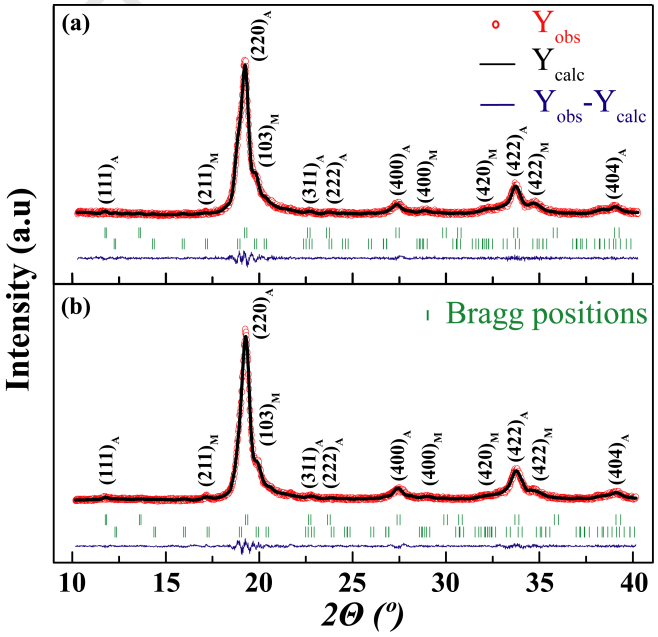

FIG. 1. X-ray powder diffraction pattern of $Ni_{50}Mn_{35-x}B_xIn_{15}$ (x=1 (a) , x= 1.5 (b)) at room temperature

It is reported that while heating $Ni_{50}Mn_{35}In_{15}$ shows several phase transitions; (i) at T=T_C^M a magnetic transition associated with the ferromagnetic ordering of the martensite phase, (ii) at T=T_M a magnetostructural phase transition, and (iii) at T=T_C^A a ferromagnetic-paramagnetic transition at the Curie temperature (T_C) of the austenitic phase[39,17].

Figure 2 (a)-(b) shows the DSC curves of B1 and B1.5 samples, respectively. It is clear that both samples show reversible martensitic phase transformation. The

TABLE I. Unit cell parameters with refinement results of $Ni_{50}Mn_{35-x}B_xIn_{15}$ (x=1, 1.5)

x	*Type*	a (Å)	b (Å)	c (Å)	V (Å)	R_p	R_{wp}	χ^2
1.0	$L2_1$	6.006 (3)	6.006 (3)	6.006 (3)	216.724	6.2	8.5	1.3
	$L1_0$	5.703 (2)	5.703 (2)	6.656 (3)	216.503			
1.5	$L2_1$	5.996 (3)	5.996 (3)	5.996 (3)	215.16	6.0	8.3	1.5
	$L1_0$	5.676 (3)	5.676 (3)	6.632 (3)	213.70			

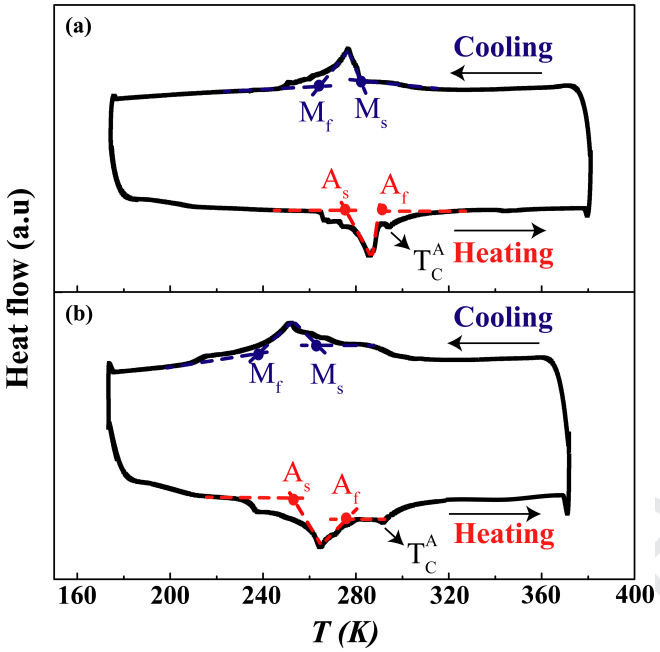

FIG. 2. DSC curves of $Ni_{50}Mn_{35-x}B_xIn_{15}$ (x=1.0 (a) and 1.5 (b)) samples

large endothermic/exothermic peaks are related to the latent heat of the first-order magnetostructural transitions. We have determined the martensite start (M_s) and finish (M_f), austenite start (A_s) and finish (A_f) temperatures, and transformation entropy (ΔS) and listed in Table 2. Meanwhile, throughout the transition, we observed that the DSC curves of the samples did not change monotonously. Comparably, a broad transition behavior was also observed for similar B doped NiMnIn alloys[17,35]. This can be attributed to the compositional in homogeneity and internal stress caused by the microstructural defects such as coexistence of different phases or boundary motion[40]. Furthermore, thermal hysteresis values computed from DSC thermograms were 16 K and 23 K , respectively for B1 and B1.5 via ΔT_{hys}=((A_s+A_f)/2 - (M_s+M_f)/2). According to DSC data, forward transformation entropy change across MST (ΔS_M) was computed 46 J $kg^{-1}K^{-1}$ and 27 J $kg^{-1}K^{-1}$, while for the reverse transformations it was computed to be (ΔS_A) 34 J $kg^{-1}K^{-1}$ and 22 J $kg^{-1}K^{-1}$, for B1 and B1.5 samples, respectively. The reverse and forward transformations entropy changes of B1.5 samples are close to each other but not for B1 sample. This difference might be due to the different energy barriers of the forward and reverse transformations or dissipating processes accompanying the transformation and phase front motion due to the incompatibility between the transforming phases are different for forward and reverse transformation[41].

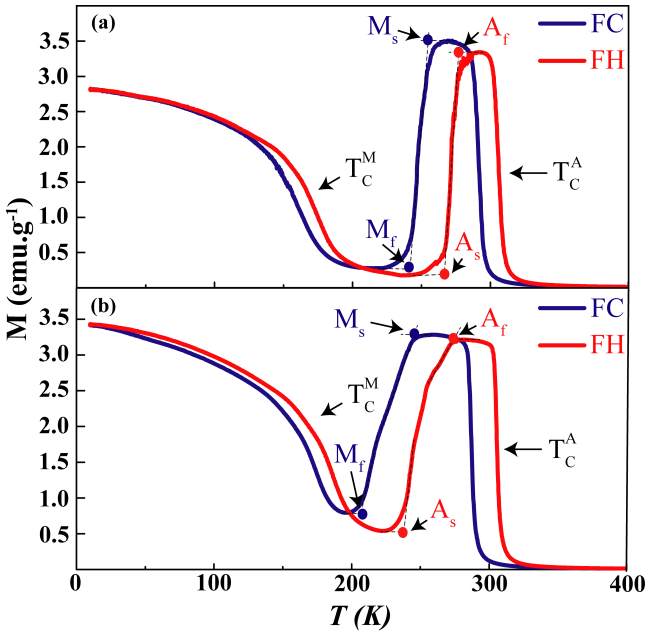

FIG. 3. 10 mT thermomagnetization curves of $Ni_{50}Mn_{35-x}B_xIn_{15}$ (x=1.0 (a) and 1.5 (b)) samples

Figure 3 (a)-(b) shows temperature dependent magnetization curves of B1 and B1.5 samples at low magnetic field of 10 mT, respectively. According to these results, at 150 K there is the Curie temperature for the martensite phase T_C^M. With further heating, we observed a first order reverse MST between 270 - 300 K. Afterwards, at T_C^A=310 K we observed ferromagnetic-paramagnetic phase transition. The same scenario is valid for B1.5 sample, which differs the transition temperatures except for T_C^M and T_C^A. It is clear that the martensitic transformation temperatures decrease as the B content increases. We observed ferromagnetic ordering of the martensitic phase around 150 K for B1.5 similar to B1 sample. However, the nature of the martensitic structural transition was different. We observed that the MST occurred in a wider temperature range. For heating, reverse martensitic structural transition occurred between 230 - 280 K. In addition, we observed a fluctuation in magnetization data around MST for B1.5 sample which was absent in B1 sample. We also observed that the hysteresis simultaneously increased as B content increased. The thermal hysteresis of B1 computed as A_f-M_s= 20 K while for B1.5 it was 30 K. Therefore, a small amount of B in the Mn position induces a non linear-temperature decrease of the MST which is in line with a previous study where B substitution for In was investigated[17]. However, there exist discrepancy between transition temperatures determined from DSC and M(T) data given in Table 2. The

TABLE II. The transformation temperatures determined from DSC and 100 Oe M(T) data of $Ni_{50}Mn_{35-x}B_xIn_{15}$ (x=1,1.5) alloys.

x	$Measurement$	M_s (K)	M_f (K)	A_s (K)	A_f (K)	T_M (K)	T_A (K)	ΔT_{hys} (K)	$A_f - M_f$ (K)
1.0	DSC	276	259	271	285	265	281	16	26
	$M(T)$	259	237	265	277	251	268	23	40
1.5	DSC	260	238	254	277	246	269	23	39
	$M(T)$	245	207	233	272	220	258	26	65

discrepancy between these two data may have resulted from different specimen sizes, slightly different compositions, or different heating and cooling rates. Moreover, it is reported that substituting B for Mn activates at least two mechanisms: a decrease in crystal cell volume, and a distortion of the local atomic environment. The smaller crystal cell volume can stabilize the martensitic phase and, as a consequence, increases T_M. However, the local distortion in electronic structure, alloys with x $\leq$ 1.0 may stabilize in the austenitic phase and therefore shift T_M to lower temperature[17].

In addition, it was reported that co-existence of two magnetic phases near T_C, one of them is antiferromagnetic low temperature martensitic. As well, the other one is non-ferromagnetic (NFM) high temperature fractions which can induce cluster-like ferromagnetic structures, that is pinned in the external magnetic field direction[35]. Furthermore, it is reported the application of magnetic field can destroy the pinning and release the ferromagnetism, and therefore increase the interval of temperature stability of the austenite phase. Therefore, the splitting of the M(T) curves near T_C of austenite phase might be due to the pinned ferromagnetic structures leading to increased temperature stability of the austenite phase[35].

Figure 4 (a)-(b) shows thermo-magnetization curves M(T) of B1 and B1.5 samples respectively. M(T) measurements were performed in the temperature range 10 K $\leq$ T $\leq$ 400 K. The rapid decrease or increase of the magnetization with respect to temperature variation have assigned to the phase transformation from austenite to martensite phase, where the minimum magnetization has reached with following slight increase upon decreasing temperature. Similar to the low magnetic field thermomagnetization curve, we observed three phase transitions: T_C^M, T_M, and T_C^A. However, these temperatures shifted to lower temperatures as the applied magnetic field increased. Since external magnetic field stabilizes the phase with higher magnetization (austenite phase in this study), the transition shifted to lower temperatures. In addition, we observed that 5 T was not sufficient to saturate the magnetization and the minimum value of magnetization was decreased with increasing the magnetic field, which is the sign of ferrimagnetic ordering of the martensite phase[42]. Therefore, ferrimagnetic to ferromagnetic transition occurred the martensite phase T_C^M. In contrast, for the austenite phase paramangetic to ferromagnetic transition occurred shown as T_C^A in Fig 4. The martensitic transformation temperatures under magnetic field of 0.5 T, 1 T, 3 T, and 5 T, are plotted in Fig. 4 (c)-(d) for B1 and B1.5, respectively. Furthermore, we observed that B1.5 sample showed similar behavior for the low magnetic fields to the B1 sample. However, unlike the B1 sample, we observed fluctuation in B1.5 sample thermomagnetization data that became prominent for higher magnetic fields. Such behavior might be due to the existence of intermediate phase or enhanced chemical pressure upon increasing B addition during synthesizing procedure[43]. The characteristic temperatures, M_f, A_f, M_s, and A_s, linearly decreased with the applied magnetic field and it was given in Figure 4 (c)-(d). It was previously reported that transition temperatures decreased by 8 K/T for $Ni_{45}Mn_{50}In_{14.25}B_{0.75}$, which is higher as compared to our case here. The different rate of change in heating and cooling direction also points to the non-linear change of shift of the magnetostructural transition. The hysteresis of both alloys is almost independent of the magnetic field. As one can see the nature of the transition is similar to the low applied magnetic field and high applied magnetic fields, thereby, a strong magnetic field was not sufficient to suppress the magnetic properties observed in the low magnetic field. It was suggested that this behavior is related to the presence of nearly "disordered" long-range ferromagnetism in the austenitic phase[17]. Thus, the application of a magnetic field weakly affects the temperature of magnetostructural transitions. The shift in the transition temperature with the magnetic field is accounted for by the Claussius-Clapeyron equation: $\Delta T \approx \Delta M / \Delta S \, \Delta H$, where ΔM and ΔS are the differences in the magnetization and entropy between the austenite and martensite phases, respectively. ΔS of the B1 and B1.5 samples are calculated from the average entropy data obtained from DSC as ΔS=36.5 J/kg K and 28 J/kg K, respectively. Using the equation above with ΔH= 5 T and ΔM for the B1 and B1.5 samples as 60 emu/g and 45 emu/g, respectively. The corresponding ΔT are calculated as 8.2 K and 8.0 K, for B1 and B1.5, respectively.

Moreover, Fig. 5 (a)-(b) illustrates the magnetic field dependent magnetization curves at several temperatures increasing and decreasing fields up to 5 T. For both samples, as the temperature approached to the MST, magnetization increased. However, magnetization decreased for the temperatures away from MST. The critical field of some of the curves was within a certain temperature range corresponding to the onset of typical metamagnetic behavior. The critical field of the direct meta-

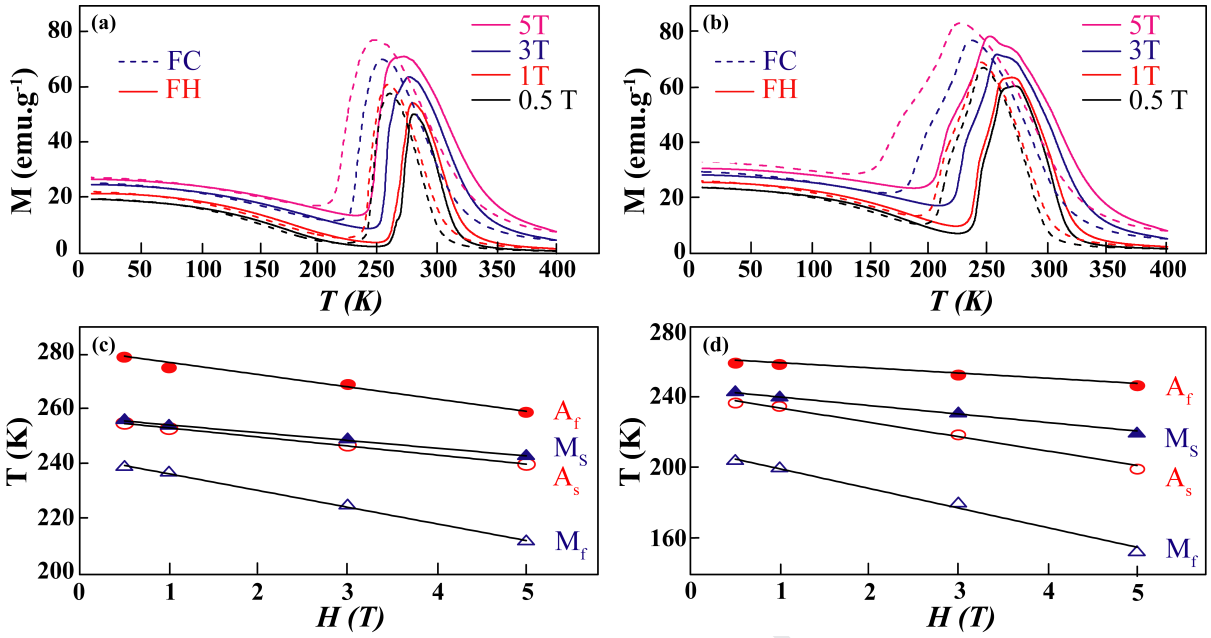

FIG. 4. (a)-(b) Thermomagnetization curves of $Ni_{50}Mn_{35-x}B_xIn_{15}$ (x=1.0 and 1.5) samples, respectively. (c)-(d) The martensitic transformation temperatures determined from the M(T) curves of (x=1 .0 and 1.5) samples, respectively. Lines correspond to linear regression to the data.

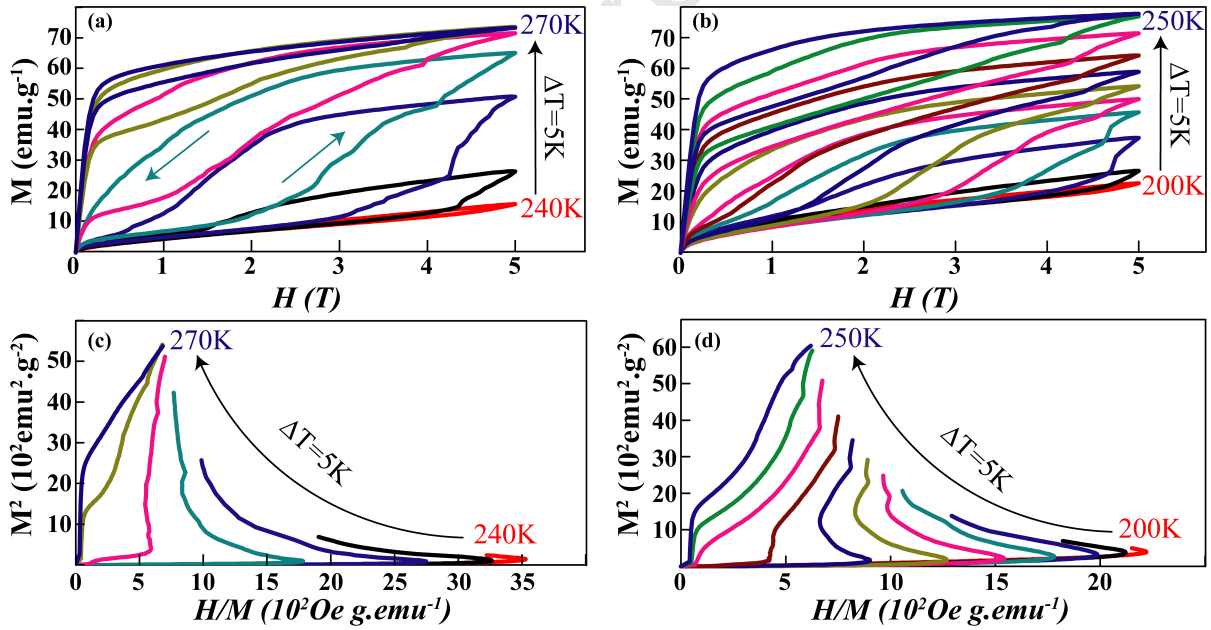

FIG. 5. (a)-(b) Isothermal magnetization curves of $Ni_{50}Mn_{35-x}B_xIn_{15}$ (x=1.0 and 1.5) samples, respectively. (c)-(d) Corresponding Arrott plots (i.e., M^2 vs. H/M) derived from the M (H) curves at different temperatures of (x= 1.0 and 1.5) samples, respectively.

magnetic transition decreases with increasing temperature. Also, we observed magnetic hysteresis with a maximum 2.8 T at 250 K for B1 sample. However, for B1.5 sample the magnetic hysteresis was smaller than B1 sample. Thereby, these observations indicate the onset of a magnetic field induced transformation (MFIT) from the martensitic phase to the austenitic phase.

According to the Banerejee criteria[44,45], a positive slope of the M^2 vs. H/M curves corresponds to the second-order phase transition; meanwhile the S-shaped (negative slope) is associated with the first order transition. To illustrate the nature of MFIT we plotted the

Arrott plots (M^2 vs. H/M) that derived from corresponding M-H curves shown in Fig. 5 (a)-(b). The negative slopes in Figs. 5 (c)-(d) confirms the MFIT and phase transition are 1^{st} order for both alloys. Moreover, we observed sharper slope for B1 sample than B1.5. Therefore, we expect a larger ΔS_M for B1 than B1.5 sample[46,47].

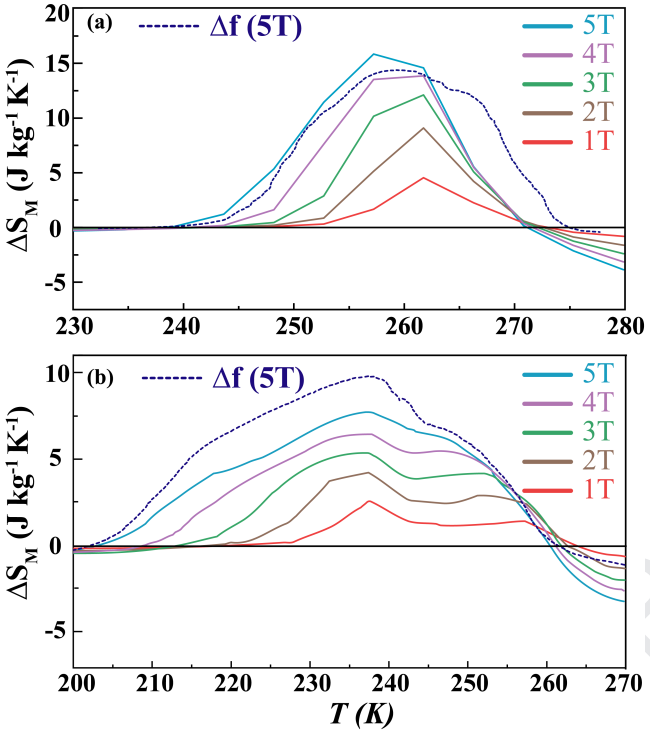

FIG. 6. Temperature dependent isothermal entropy changed under the applied magnetic field of $Ni_{50}Mn_{35-x}B_xIn_{15}$ (x=1.0 (a) and 1.5 (b)) samples, respectively

The magnetic entropy changes (ΔS_M) as a function of temperature for various applied fields (ΔH) are shown in Figure 6 (a)-(b). The ΔS_M was calculated from the magnetization isotherms using the Maxwell relation[48]. As Clauisuis-Clapeyron dictates, the higher magnetization change, the higher magnetocaloric effect. Accordingly, we observed higher ΔS_M values for B1 sample rather than B1.5 sample. Samples exhibited inverse magnetocaloric effect close to MST and conventional magnetocaloric effect at around Curie temperature due to $\Delta M/\Delta T \leq 0$. The maximum inverse magnetocaloric effect at around MST temperature for magnetic field change ΔH =5 T are ΔS = 15 J $kg^{-1}K^{-1}$ and 8 J $kg^{-1}K^{-1}$ for B1 and B1.5, respectively. The inverse nature of the magnetocaloric effect is consistent with the magnetic field stabilization of the cubic phase. Meanwhile, B1.5 sample ΔS peak originating from MST was split into two as the external field increases and is visible for ΔS_M of 4 T at 245 K. This splitting might be due to the arrested austenitic phase during the reverse field-induced MST[35]. In addition, ΔS_M of the B1.5 has a much broader temperature interval than the B1 alloy that might due to the existence of the intermediate phases where two steps of the MCE occurred during the heating direction that is seen in Fig. 6(b) as a two peaks between temperatures of 240 K and 260 K[49]. Besides, one can predict that the maximum conventional magnetecaloric effect around to be 5 J $kg^{-1}K^{-1}$ for the second order ferromagnetic-paramagnetic transition at T_C for both samples.

A new method, namely the "fraction method" was introduced to compute the entropy change due to the application of magnetic field, in which it can be calculated from the Clausius–Clapeyron (CC) slope and isofield magnetization[50]. Thence, we computed the magnetic field-inducealculatedge (ΔS_M) with the fraction method to check results from Maxwell relation. It has been reported that total magnetization is proportional to the phase volume fraction[21,51–53]. Therefore, austenite or martensite phase fraction, f(T), can be described by using M(T) data. The phase fraction was computed following

$$f(T) = \frac{M(T) - M_M(T)}{M_A(T) - M_M(T)} \quad (1)$$

where M_M(T) was the magnetization of full martensite and M_A(T) is the magnetization of full austenite. It is known that both temperature and the magnetic field are thermodynamic analogs for driving the martensite phase transition, therefore phase fraction $f(T)$ was quantitatively estimated with thermomagnetization data obtained under different magnetic fields[45,51]. Additionally, the total entropy changes (ΔS_{tr}) across full transition was estimated by the Clausius-Clapeyron equation: ΔS_{tr} = -ΔM(dH/dT_A)[50]. In this relationship, ΔM is the difference in magnitude between the two phases at the transition temperature, dT_A/dH is the rate of change of the transition temperature during heating direction with the magnetic field. Since the phase fraction shows the phase transformation induced by the application of the magnetic field, one can combine the isothermal entropy change with the phase fraction induced by the application of magnetic field namely magnetocaloric effect as[50].

$$\Delta S_M = \Delta f.\Delta S_{tr} = (f(T, H_f) - f(T, H_i)) * \Delta M(dH/dT_A) \quad (2)$$

Finally, we have computed magnetic field induced entropy change for 5 T and shown in Figure 6 as scatter. As one can see, ΔS_M computed by Maxwell method and fraction method results are in line with each other for B1 sample. However, for B1.5 there exist little difference between ΔS_M computed by two methods. This difference might be due to fluctuations observed in M(T) data which is much prominent for higher magnetic fields. Also, it is reported that B addition might lead to enlargement of chemical pressure upon increasing B addition during synthesizing procedure[43] and existence of intermediate phase thereby fluctuations in magnetization data. This might be the reason for the difference observed in ΔS_M computation with two methods.

IV. CONCLUSION

In conclusion, the magnetic and martensitic transformation behavior of $Ni_{50}Mn_{35-x}B_xIn_{15}$ (x=1.0 and 1.5) samples were investigated. Boron has much smaller atomic radius compared with that of Mn, thereby the substitution of which for Mn shortened the distance between manganese atoms and change the magnetic properties of $Ni_{50}Mn_{35-x}B_xIn_{15}$ drastically. Magnetic field application shifted martensite transformation temperatures to lower temperatures. In addition, magnetic field application induced the magnetic field-induced phase transformation from martensite to austenite. We have calculated the magnetic field induced transition with two different methods and we observed that the calculated values of entropy change are in line with each other. Boron addition might be helpful to tune transition temperatures and we observed hysteresis increases as boron content increases. However, boron addition also leads to decrease of transition entropy and magnetocaloric effect.

* bemre@eng.ankara.edu.tr

[1] F. Birol, International Energy Agency (2018).
[2] B. Emre, O. Yıldırım, and E. Duman, Materials Research Express **6**, 076102 (2019).
[3] L. Mañosa, A. Planes, and M. Acet, Journal of Materials Chemistry A **1**, 4925 (2013).
[4] M. Pasquale, C. P. Sasso, L. Giudici, T. Lograsso, and D. Schlagel, Applied Physics Letters **91**, 131904 (2007).
[5] T. Krenke, E. Duman, M. Acet, E. F. Wassermann, X. Moya, L. Mañosa, and A. Planes, Nature Materials **4**, 450 (2005).
[6] P. O. Castillo-Villa, L. Mañosa, A. Planes, D. E. Soto-Parra, J. L. Sánchez-Llamazares, H. Flores-Zúñiga, and C. Frontera, Journal of Applied Physics **113**, 053506 (2013).
[7] R. Kainuma, Y. Imano, W. Ito, Y. Sutou, H. Morito, S. Okamoto, O. Kitakami, K. Oikawa, A. Fujita, T. Kanomata, *et al.*, Nature **439**, 957 (2006).
[8] Y. Sutou, Y. Imano, N. Koeda, T. Omori, R. Kainuma, K. Ishida, and K. Oikawa, Applied Physics Letters **85**, 4358 (2004).
[9] H. Karaca, I. Karaman, B. Basaran, D. Lagoudas, Y. Chumlyakov, and H. Maier, Scripta Materialia **55**, 803 (2006).
[10] K. Koyama, H. Okada, K. Watanabe, T. Kanomata, R. Kainuma, W. Ito, K. Oikawa, and K. Ishida, Applied Physics Letters **89**, 182510 (2006).
[11] A. K. Pathak, I. Dubenko, H. E. Karaca, S. Stadler, and N. Ali, Applied Physics Letters **97**, 062505 (2010).
[12] B. Zhang, X. Zhang, S. Yu, J. Chen, Z. Cao, and G. Wu, Applied Physics Letters **91**, 012510 (2007).
[13] A. Turabi, H. Karaca, H. Tobe, B. Basaran, Y. Aydogdu, and Y. Chumlyakov, Scripta Materialia **111**, 110 (2016).
[14] H. Karaca, I. Karaman, B. Basaran, Y. I. Chumlyakov, and H. Maier, Acta Materialia **54**, 233 (2006).
[15] H. Karaca, I. Karaman, A. Brewer, B. Basaran, Y. Chumlyakov, and H. Maier, Scripta Materialia **58**, 815 (2008).
[16] A. Vasiliev, O. Heczko, O. Volkova, T. Vasilchikova, T. Voloshok, K. Klimov, W. Ito, R. Kainuma, K. Ishida, K. Oikawa, *et al.*, Journal of Physics D: Applied Physics **43**, 055004 (2010).
[17] S. Pandey, A. Quetz, I. Rodionov, A. Aryal, M. Blinov, I. Titov, V. Prudnikov, A. Granovsky, I. Dubenko, S. Stadler, *et al.*, Journal of Applied Physics **117**, 183905 (2015).
[18] A. Pecharsky, K. Gschneidner Jr, and V. Pecharsky, Journal of Applied Physics **93**, 4722 (2003).
[19] O. Tegus, E. Brück, K. Buschow, and F. De Boer, Nature **415**, 150 (2002).
[20] S. Pandey, A. Quetz, A. Aryal, T. Samanta, I. Dubenko, S. Stadler, and N. Ali, Journal of Applied Physics **117**, 17A737 (2015).
[21] B. Emre, S. Yüce, E. Stern-Taulats, A. Planes, S. Fabbrici, F. Albertini, and L. Mañosa, Journal of Applied Physics **113**, 213905 (2013).
[22] S. Yu, Z. Liu, G. Liu, J. Chen, Z. Cao, G. Wu, B. Zhang, and X. Zhang, Applied Physics Letters **89**, 162503 (2006).
[23] I. Dubenko, T. Samanta, A. Quetz, A. Saleheen, V. N. Prudnikov, A. B. Granovsky, S. Stadler, and N. Ali, Physica Status Solidi (c) **11**, 1000 (2014).
[24] I. Dubenko, A. Pathak, S. Stadler, N. Ali, Y. Kovarskii, V. Prudnikov, N. Perov, and A. Granovsky, Physical Review B **80**, 092408 (2009).
[25] K. Ullakko, J. Huang, C. Kantner, R. O'handley, and V. Kokorin, Applied Physics Letters **69**, 1966 (1996).
[26] P. Devi, C. S. Mejía, L. Caron, S. Singh, M. Nicklas, and C. Felser, Physical Review Materials **3**, 122401 (2019).
[27] K. Priolkar, P. Bhobe, D. Lobo, S. D'Souza, S. Barman, A. Chakrabarti, and S. Emura, Physical Review B **87**, 144412 (2013).
[28] E. Şaşıoğlu, L. Sandratskii, and P. Bruno, Physical Review B **77**, 064417 (2008).
[29] V. Sokolovskiy, V. Buchelnikov, S. Taskaev, V. Khovaylo, M. Ogura, and P. Entel, Journal of Physics D: Applied Physics **46**, 305003 (2013).
[30] M. Kaya, M. Cicek, I. Dincer, and Y. Elerman, Journal of Magnetism and Magnetic Materials **442**, 429 (2017).
[31] M. Kaya, S. Yildirim, E. Yüzüak, I. Dincer, R. Ellialtioglu, and Y. Elerman, Journal of Magnetism and Magnetic materials **368**, 191 (2014).
[32] Z. Li, J. Yang, D. Li, Z. Li, B. Yang, H. Yan, C. F. Sánchez-Valdés, J. L. S. Llamazares, Y. Zhang, C. Esling, *et al.*, Advanced Electronic Materials **5**, 1800845 (2019).
[33] B. R. Gautam, I. Dubenko, A. K. Pathak, S. Stadler, and N. Ali, Journal of Physics: Condensed Matter **20**, 465209 (2008).
[34] Y. Aydogdu, A. S. Turabi, M. Kok, A. Aydogdu, H. Tobe, and H. E. Karaca, Applied Physics A **117**, 2073 (2014).
[35] S. Pandey, A. Quetz, A. Aryal, I. Dubenko, D. Mazumdar, S. Stadler, and N. Ali, Journal of Magnetism and Magnetic Materials **444**, 98 (2017).
[36] J. Rodríguez-Carvajal, Physica B **192**, 55 (1993).
[37] "Mention of commercial equipment is provided only for completely specifying the experimental conditions. it does not imply recommendation or endorsement by the authors

or their institutions.".
[38] L. Caron, Z. Ou, T. Nguyen, D. C. Thanh, O. Tegus, and E. Brück, Journal of Magnetism and Magnetic Materials **321**, 3559 (2009).
[39] A. Quetz, Y. S. Koshkid'ko, I. Titov, I. Rodionov, S. Pandey, A. Aryal, P. J. Ibarra-Gaytan, V. Prudnikov, A. Granovsky, I. Dubenko, *et al.*, Journal of Alloys and Compounds **683**, 139 (2016).
[40] O. Gutfleisch, T. Gottschall, M. Fries, D. Benke, I. Radulov, K. P. Skokov, H. Wende, M. Gruner, M. Acet, P. Entel, *et al.*, Philosophical Transactions of the Royal Society A: Mathematical, Physical and Engineering Sciences **374**, 20150308 (2016).
[41] N. M. Bruno, Y. J. Huang, C. L. Dennis, J. G. Li, R. D. Shull, J. H. Ross, Y. I. Chumlyakov, and I. Karaman, Journal of Applied Physics **120**, 075101 (2016).
[42] L. Bennett, V. Provenzano, R. Shull, I. Levin, E. Della Torre, and Y. Jin, Journal of Alloys and Compounds **525**, 34 (2012).
[43] Y. Wu, S. Guo, S. Yu, H. Cheng, R. Wang, H. Xiao, L. Xu, R. Xiong, Y. Liu, Z. Xia, *et al.*, Scientific Reports **6**, 26068 (2016).
[44] B. Banerjee, Physics Letters **12**, 16 (1964).
[45] B. Emre, I. Dincer, Y. Elerman, and S. Aksoy, Solid State Sciences **22**, 1 (2013).
[46] Y. Zhang, Q. Zheng, W. Xia, J. Zhang, J. Du, and A. Yan, Scripta Materialia **104**, 41 (2015).
[47] Y. Qu, D. Cong, X. Sun, Z. Nie, W. Gui, R. Li, Y. Ren, and Y. Wang, Acta Materialia **134**, 236 (2017).
[48] A. Tishin and Y. Spichkin, Condensed Matter Physics, Institute of Physics, Publishing Ltd (2003).
[49] Z. Li, K. Xu, Y. Zhang, C. Tao, D. Zheng, and C. Jing, Scientific Reports **5**, 1 (2015).
[50] K. Xu, Z. Li, Y.-L. Zhang, and C. Jing, Physics Letters A **379**, 3149 (2015).
[51] E. Stern-Taulats, P. O. Castillo-Villa, L. Mañosa, C. Frontera, S. Pramanick, S. Majumdar, and A. Planes, Journal of Applied Physics **115**, 173907 (2014).
[52] V. Basso, C. P. Sasso, K. P. Skokov, O. Gutfleisch, and V. V. Khovaylo, Physical Review B **85**, 014430 (2012).
[53] P. J. Shamberger and F. Ohuchi, Physical Review B **79**, 144407 (2009).

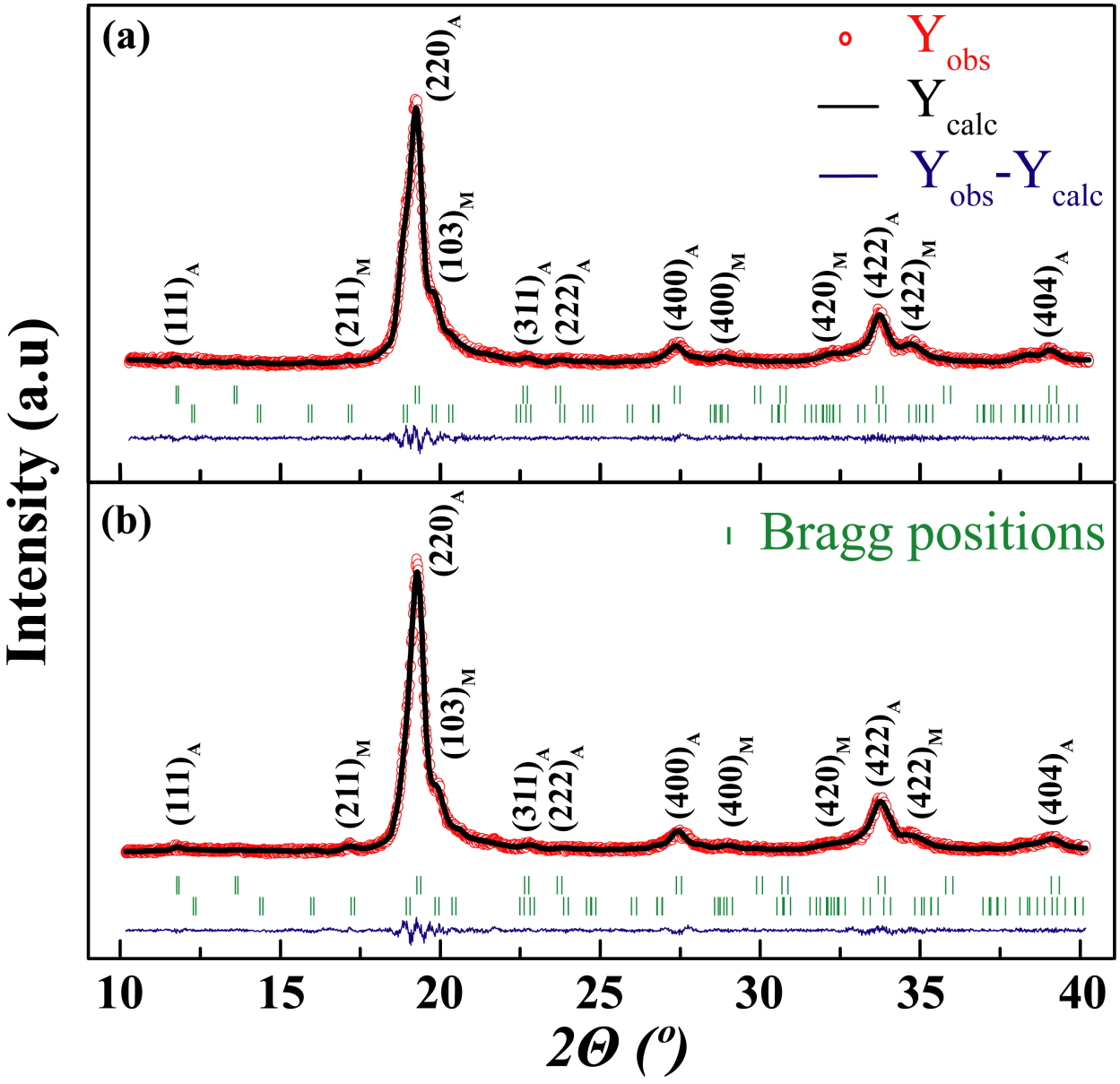
(a)
(b)
Y obs
Y calc
Y obs-Y calc
Bragg positions
(111)A
(211)M
(220)A
(103)M
(311)A
(222)A
(400)A
(400)M
(420)M
(422)A
(422)M
(404)A
Intensity (a.u)
10
15
20
25
30
35
40
2Θ (°)

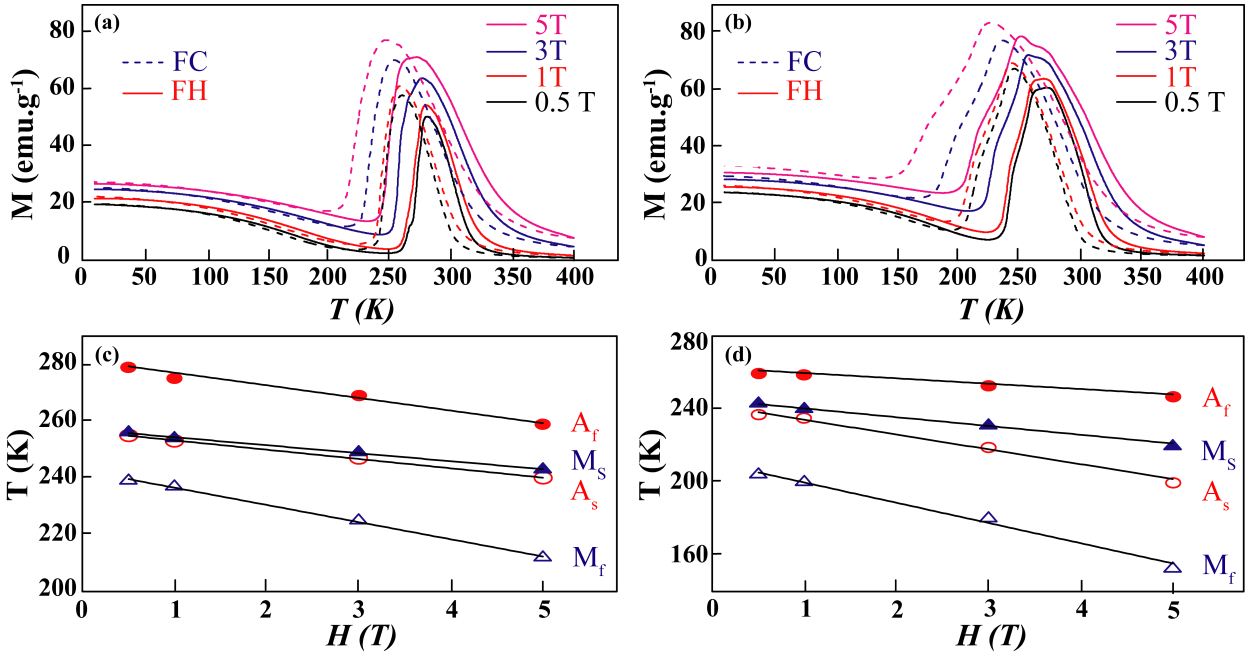

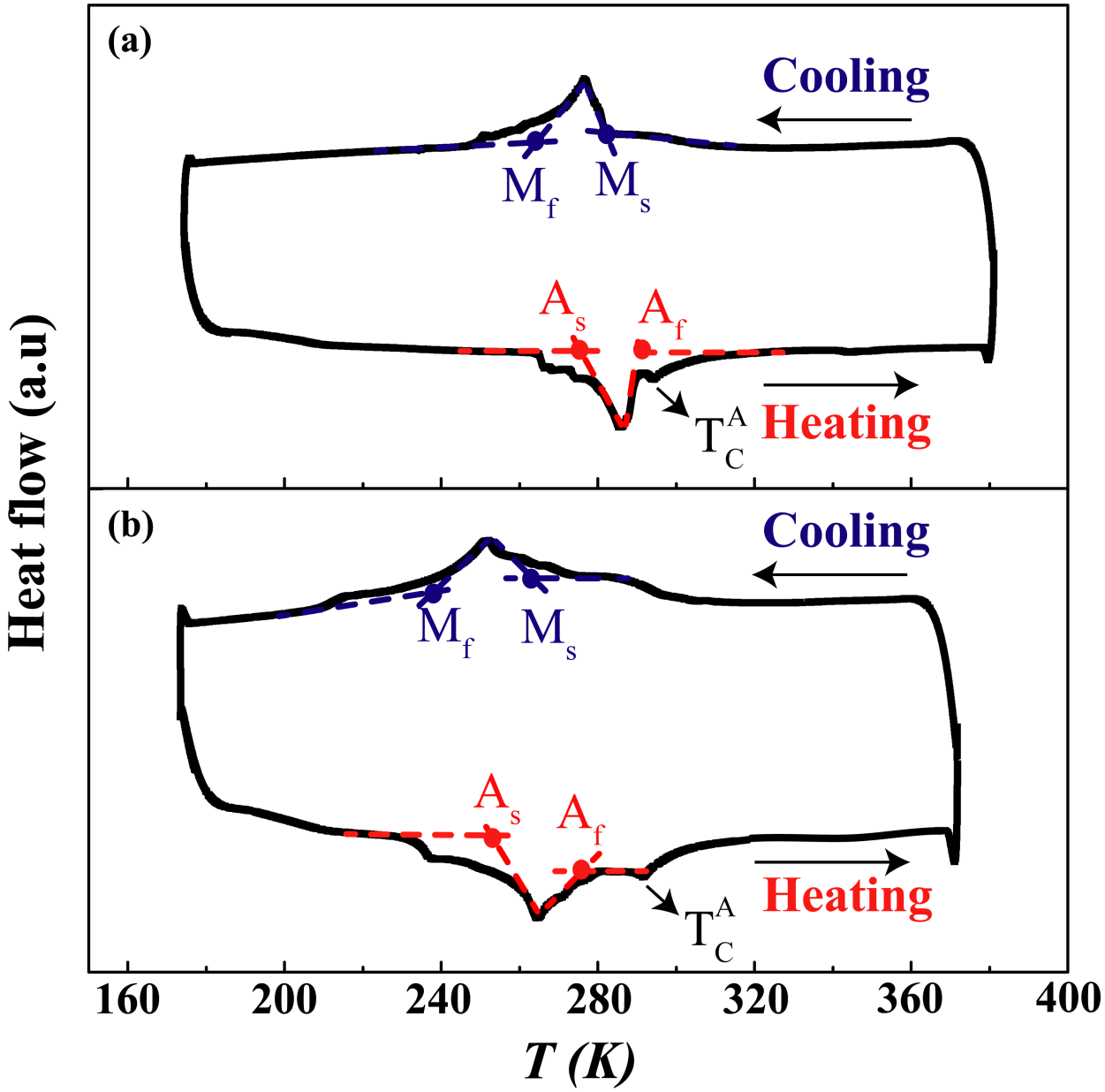
(a)
Cooling
M_f
M_s
A_s
A_f
T_C^A
Heating
(b)
Cooling
M_f
M_s
A_s
A_f
T_C^A
Heating
Heat flow (a.u)
160
200
240
280
320
360
400
T (K)

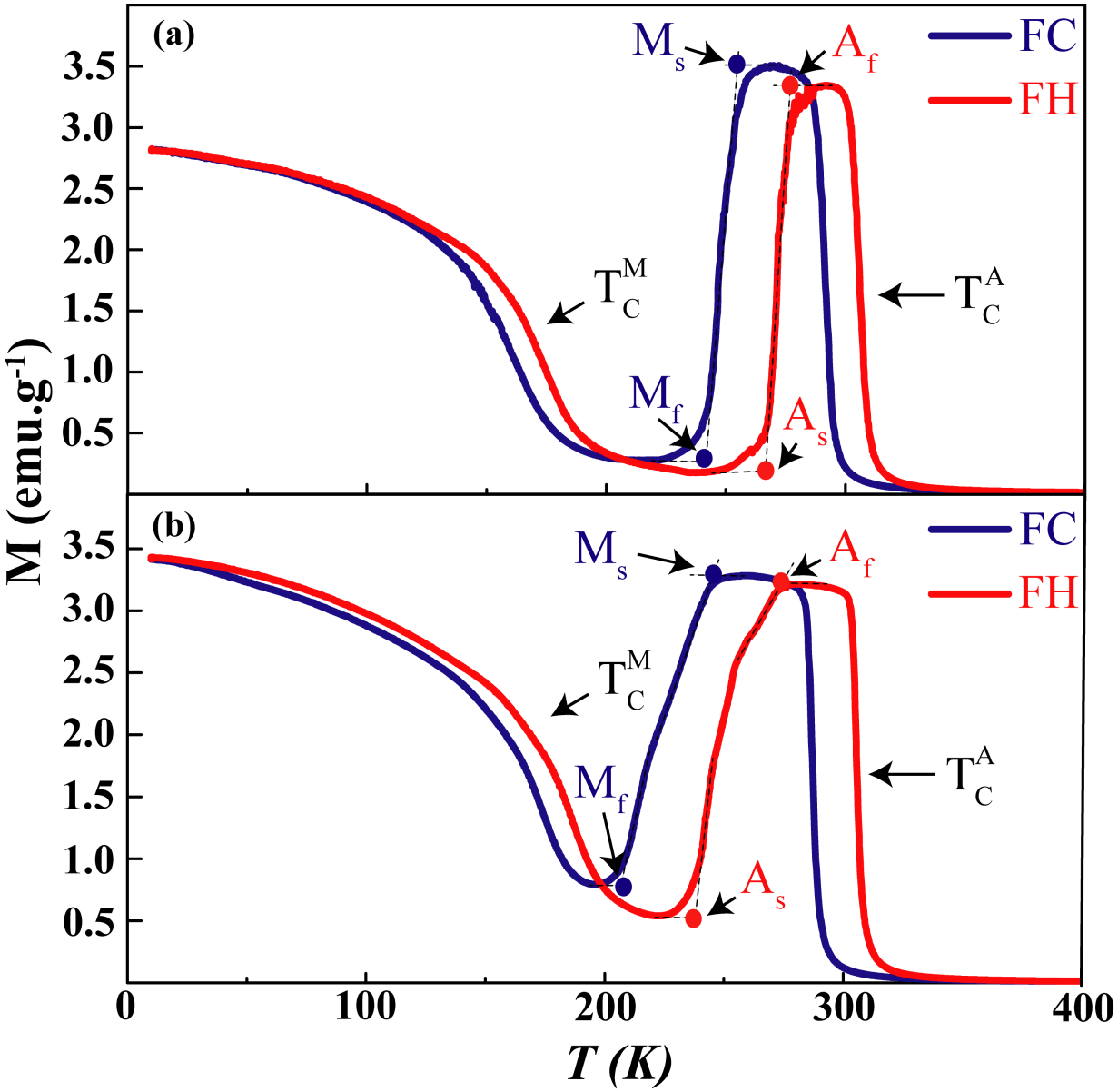
(a)
(b)
FC
FH
M_s
A_f
M_f
A_s
T_C^M
T_C^A
M (emu.g^{-1})
T (K)
0
100
200
300
400
0.5
1.0
1.5
2.0
2.5
3.0
3.5

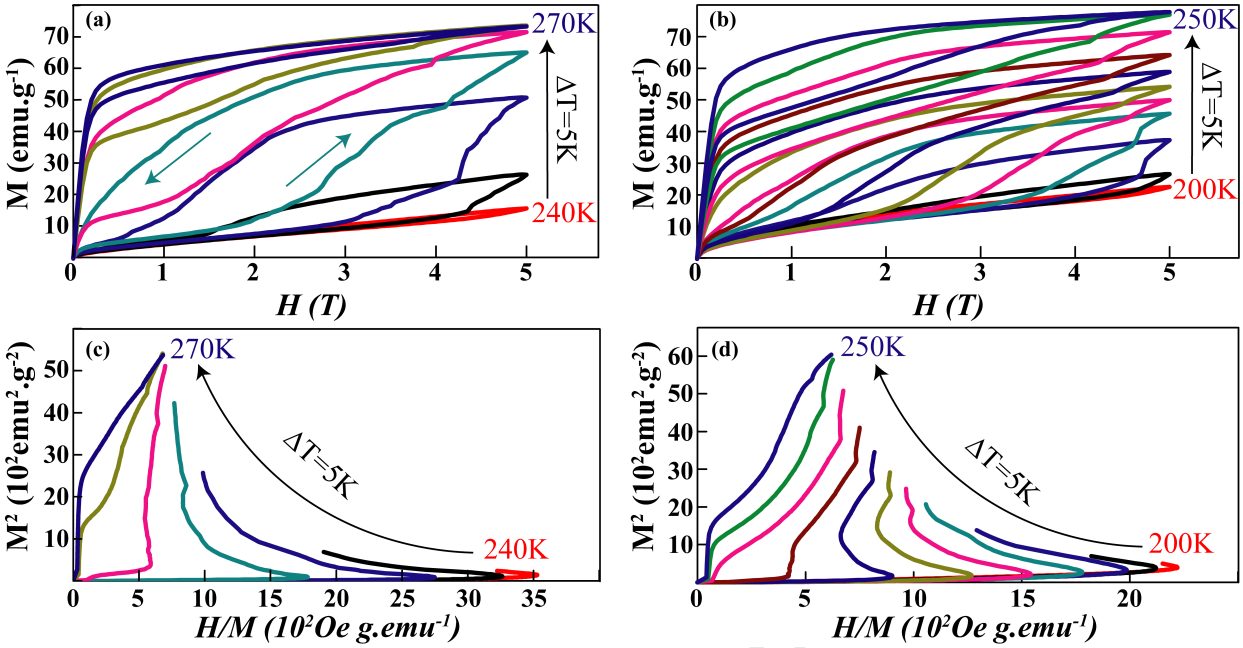

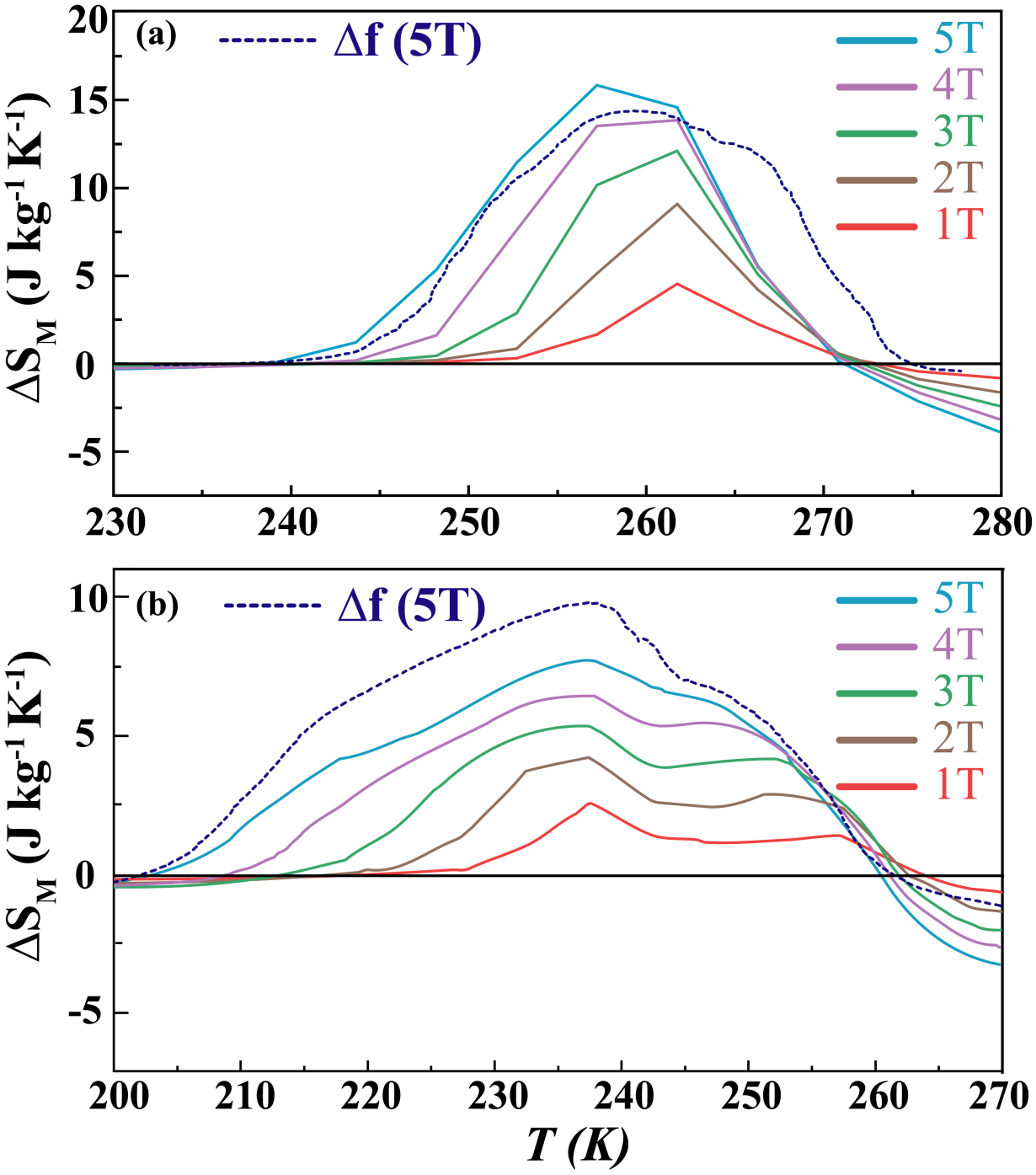
(a)
Δf (5T)
5T
4T
3T
2T
1T
ΔS_M (J kg^-1 K^-1)
20
15
10
5
0
-5
230
240
250
260
270
280
(b)
Δf (5T)
5T
4T
3T
2T
1T
ΔS_M (J kg^-1 K^-1)
10
5
0
-5
200
210
220
230
240
250
260
270
T (K)

Highlights

- Boron substitution is an effective way to tune martensitic transitions temperatures.
- Both alloys have moderate ΔM and thermal hysteresis across martensitic transformation.
- Transition entropy, magnetocaloric effect decreased meanwhile thermal hysteresis increased with B substitution.
- Moderate magnetocaloric effect is obtained and validated by two different methods.

Declaration of competing interest

The authors declare that they have no competing interests.

CRediT authorship contribution statement

M.M.Cicek: Investigation, Writing - original draft. **S. Saritas:** Investigation. **O. Yildirim:** Investigation **B. Emre:** Writing - original draft, Supervision.